Effective Diversity of OTFS Modulation

P. Raviteja, Yi Hong, Emanuele Viterbo, and Ezio Biglieri

***Abstract*—Orthogonal time frequency space (OTFS) modulation, which encodes information symbols in the delay–Doppler domain, offers a promising solution to the problem of high Doppler sensitivity of orthogonal frequency division multiplexing (OFDM) transmission. In this letter we study the diversity of OTFS assuming rectangular waveforms and a delay–Doppler channel with two paths. After introducing the concept of *effective diversity* (ED), which we argue to be more significant than "standard" diversity in the case of a large number of transmitted symbols, we examine the conditions under which OTFS achieves full ED for QAM symbols. We validate our analytical results through numerical simulations, which show that OTFS practically achieves full ED with sufficiently large signal constellations.**

***Index Terms*—Delay–Doppler channel, diversity, OTFS.**

I. Introduction

A SIMPLE and effective way of evaluating symbol error rates in digital communications is based on the concept of pairwise error probabilities (PEPs) [1], whose sum over all transmitted signal pairs yields an upper bound to said rate. With Rayleigh fading channels, performance is often expressed using a single parameter, called *diversity*, representing the minimum slope of the PEP-vs.-SNR curves across all signal pairs. This turns out to be the slope of the actual symbol error probability for high SNR. Now, in the case of a large number of transmitted signals and intermediate SNR, diversity may not be a meaningful parameter, as a large majority of PEP curves may exhibit a slope much steeper than the minimum. In these conditions, we advocate the use of an *effective diversity* (ED), which accounts for the slope of the majority of PEP curves rather than the minimum one. In this letter, we focus on studying this parameter for orthogonal time frequency space (OTFS) modulation, which is a recently proposed waveform for high Doppler channels [2], [3]. Some other works on OTFS may be found in [4]–[14].

Recently, in [8], the authors analyzed the conventional diversity of OTFS for ideal bi-orthogonal waveforms and showed that it is one. However, this analysis does not reflect the PEP values at practical SNR's and also it is not valid for practical waveforms. In this letter, we study the performance of OTFS using ED with practical rectangular waveforms and operating over a delay–Doppler channel with two paths. ED is derived, and numerical simulations are used to validate our results.

Notations: Scalars, vectors, and matrices are denoted a, $\mathbf{a}$, and $\mathbf{A}$, respectively. $\mathbf{A}^\dagger$ and $\mathbf{A}^i$ denote Hermitian transpose and i^{th} power of $\mathbf{A}$. We write $\mathbf{a} = \mathrm{vec}(\mathbf{A})$ for the column-wise vectorization of matrix $\mathbf{A}$. Symbols $\mathbf{a}(i)$ and $\mathbf{A}(i, j)$ denote the i^{th} element of $\mathbf{a}$ and $(i, j)^{th}$ element of $\mathbf{A}$, respectively. Further, $\mathbf{A} = \mathrm{diag}[a_0, \ldots, a_{N-1}]$ denotes a diagonal matrix of size N with $\{a_0, \ldots, a_{N-1}\}$ as its diagonal elements. $\mathbf{I}_N$ is the identity matrix of size N, and $\mathbf{F}_N = \{\frac{1}{\sqrt{N}} e^{2\pi jkl/N}\}_{k,l=0}^{N-1}$ and $\mathbf{F}_N^\dagger$ are the N-point DFT and the IDFT matrices, respectively. Symbol $\otimes$ denotes Kronecker product, and $\mathcal{CN}(\mathbf{0}, N_0\mathbf{I}_N)$ an i.i.d. Gaussian random vector with mean $\mathbf{0}$ and covariance matrix $N_0\mathbf{I}_N$. Notation $[\cdot]_N$ denotes mod-N operation, and $\gcd(a, b)$ the greatest common divisor of a and b. Further, $\mathbf{Z}$ and $\mathbf{Z}[j]$ denote the set of integers and the number field whose elements have the form $a + bj$, with a and b integers, respectively. Finally, $\mathbf{Q}(e^{-j2\pi\frac{1}{N}})$ denotes the cyclotomic field obtained by adjoining an N-th root of unity to the set of rational numbers.

II. System Model

We consider OTFS modulation with one transmit and one receive antenna. Let $\mathbf{X} \in \mathbb{A}^{M\times N}$ denote the two-dimensional (QAM) information symbols in the delay–Doppler domain, where the QAM alphabet $\mathbb{A} \in \{a_0, \ldots, a_{Q-1}\}$. Note that $\mathbb{A} \subset \mathbf{Z}[j]$. Assuming rectangular waveforms, the OTFS transmitted signal can be written as [5]

$$\mathbf{s} = \mathrm{vec}\Big(\mathbf{F}_M^\dagger(\mathbf{F}_M\mathbf{X}\mathbf{F}_N^\dagger)\Big) = (\mathbf{F}_N^\dagger \otimes \mathbf{I}_M)\mathbf{x} \tag{1}$$

where $\mathbf{x} \triangleq \mathrm{vec}(\mathbf{X}) \in \mathbb{A}^{MN}$. For efficient FFT implementation, we assume M and N are powers of 2.

The received signal can be put in the form [5]

$$\mathbf{r} = \mathbf{H}\mathbf{s} + \mathbf{w}, \tag{2}$$

where, under the assumption that the channel admits a P-path sparse representation as described in [6], $\mathbf{H}$ is the $MN \times MN$ channel matrix

$$\mathbf{H} = \sum_{i=1}^{P} h_i \mathbf{\Pi}^{l_i} \mathbf{\Delta}^{k_i}, \tag{3}$$

with $\mathbf{\Pi}$ the permutation matrix (forward cyclic shift), $\mathbf{\Delta}$ the $MN \times MN$ matrix $\mathbf{\Delta} \triangleq \mathrm{diag}[z^0, z^1, \ldots, z^{MN-1}]$, $z \triangleq e^{\frac{j2\pi}{MN}}$, and $\mathbf{w} \sim \mathcal{CN}(\mathbf{0}, N_0\mathbf{I})$.

Manuscript received September 12, 2019; accepted November 2, 2019. Date of publication November 6, 2019; date of current version February 7, 2020. The work of P. Raviteja, Y. Hong, and E. Viterbo was supported by the Australian Research Council through the Discovery Project under Grant DP160100528. The work of E. Biglieri was supported by the European Research Council through the H2020 Framework Programme/ERC under Grant 694974. The associate editor coordinating the review of this article and approving it for publication was S. K. Mohammed. *(Corresponding author: Emanuele Viterbo.)*

P. Raviteja, Y. Hong, and E. Viterbo are with ECSE Department, Monash University, Clayton, VIC 3800, Australia (e-mail: raviteja.patchava@monash.edu; yi.hong@monash.edu; emanuele.viterbo@monash.edu).

E. Biglieri is with the Department of Information and Communication Technologies, Universitat Pompeu Fabra, 08018 Barcelona, Spain (e-mail: ezio.biglieri@gmail.com).

Digital Object Identifier 10.1109/LWC.2019.2951758

After OTFS processing, the received signal in delay–Doppler domain becomes

$$\begin{aligned}\mathbf{y} &= (\mathbf{F}_N \otimes \mathbf{I}_M)\mathbf{H}(\mathbf{F}_N^{\dagger} \otimes \mathbf{I}_M)\mathbf{x} + (\mathbf{F}_N \otimes \mathbf{I}_M)\mathbf{w} \\ &= \mathbf{H}_{\text{eff}}\mathbf{x} + \widetilde{\mathbf{w}} \end{aligned} \tag{4}$$

where $\mathbf{H}_{\text{eff}} \triangleq (\mathbf{F}_N \otimes \mathbf{I}_M)\mathbf{H}(\mathbf{F}_N^{\dagger} \otimes \mathbf{I}_M)$ is the *effective channel matrix*, and $\widetilde{\mathbf{w}} = (\mathbf{F}_N \otimes \mathbf{I}_M)\mathbf{w}$ the noise vector.

In order to study the diversity of OTFS, we use the following two observations from our earlier work [5], [6].

Observation 1: The received signal $\mathbf{y}$ in (4) can be written as [6]

$$\mathbf{y} = \sum_{i=1}^{P} h_i(\mathbf{F}_N \otimes \mathbf{I}_M)\mathbf{\Pi}^{l_i}\mathbf{\Delta}^{k_i}(\mathbf{F}_N^{\dagger} \otimes \mathbf{I}_M)\mathbf{x} + \widetilde{\mathbf{w}} = \mathbf{\Phi}(\mathbf{x})\mathbf{h} + \widetilde{\mathbf{w}}$$

where $\mathbf{h} = [h_1, h_2, \ldots, h_P]$ is a $P \times 1$ vector of i.i.d. complex Gaussian random variables, and $\mathbf{\Phi}(\mathbf{x})$ is the $MN \times P$ concatenated matrix

$$\mathbf{\Phi}(\mathbf{x}) = [\underbrace{\mathbf{\Xi}_1}_{MN\times MN}\ \underbrace{\mathbf{x}}_{MN\times 1}\ |\ldots|\ \underbrace{\mathbf{\Xi}_P}_{MN\times MN}\ \underbrace{\mathbf{x}}_{MN\times 1}]$$

and $\mathbf{\Xi}_i \triangleq (\mathbf{F}_N \otimes \mathbf{I}_M)\mathbf{\Pi}^{l_i}\mathbf{\Delta}^{k_i}(\mathbf{F}_N^{\dagger} \otimes \mathbf{I}_M)$.

The conditional pairwise error probability for the above system can be written as

$$\begin{aligned}P(\mathbf{x} \to \hat{\mathbf{x}}\,|\,\mathbf{h}) &= \mathbb{P}(\|\mathbf{y} - \mathbf{\Phi}(\hat{\mathbf{x}})\mathbf{h}\|^2 < \|\mathbf{y} - \mathbf{\Phi}(\mathbf{x})\mathbf{h}\|^2\,|\,\mathbf{h}) \\ &= \mathcal{Q}\left(\frac{\|[\mathbf{\Phi}(\hat{\mathbf{x}}) - \mathbf{\Phi}(\mathbf{x})]\mathbf{h}\|}{\sqrt{2N_0}}\right)\end{aligned}$$

where $\mathcal{Q}$ is the Gaussian tail function.

Now, using the Chernoff upperbound, the pairwise error probability becomes

$$P(\mathbf{x} \to \hat{\mathbf{x}}) \le \mathbb{E}_{\mathbf{h}} \exp\left(\frac{-\|\mathbf{\Phi}(\boldsymbol{\delta})\mathbf{h}\|^2}{4N_0}\right)$$

where

$$\mathbf{\Phi}(\boldsymbol{\delta}) = \mathbf{\Phi}(\hat{\mathbf{x}}) - \mathbf{\Phi}(\mathbf{x}) = [\mathbf{\Xi}_1\boldsymbol{\delta}|\cdots|\mathbf{\Xi}_P\boldsymbol{\delta}] \tag{5}$$

and $\boldsymbol{\delta} = \hat{\mathbf{x}} - \mathbf{x}$ is the codeword difference vector. Note that $\boldsymbol{\delta} \subset \mathbf{Z}[j]^{MN\times 1}$.

Assuming $\mathbf{h} \sim \mathcal{CN}(\mathbf{0}, \mathbf{I})$ and $\mathbf{\Upsilon}(\boldsymbol{\delta}) = \mathbf{\Phi}^{\dagger}(\boldsymbol{\delta})\mathbf{\Phi}(\boldsymbol{\delta})$, the upper bound on the average bit error probability (BER) P_{e} can be written as [6, eq. (23)]

$$P_{\text{e}} \le \frac{1}{|Q^{MN}|}\sum_{\mathbf{x}\in\mathbb{A}^{NM}}\sum_{\hat{\mathbf{x}}\neq\mathbf{x}}\frac{d_{\text{H}}(\mathbf{x},\hat{\mathbf{x}})}{MN\log_2 Q}\left(\prod_i \lambda_i\right)^{-1}\left(\frac{1}{4N_0}\right)^{-\rho(\mathbf{x},\hat{\mathbf{x}})} \tag{6}$$

where, $MN\log_2 Q$ denotes the total number of bits transmitted in one OTFS frame, $d_{\text{H}}(\mathbf{x},\hat{\mathbf{x}})$ is the difference in number of information bits between $\mathbf{x}$ and $\hat{\mathbf{x}}$, λ_i's are the non-zero eigenvalues of $\mathbf{\Upsilon}(\boldsymbol{\delta})$, and $\rho(\mathbf{x},\hat{\mathbf{x}})$ is the number of nonzero eigenvalues of $\mathbf{\Upsilon}(\boldsymbol{\delta})$.

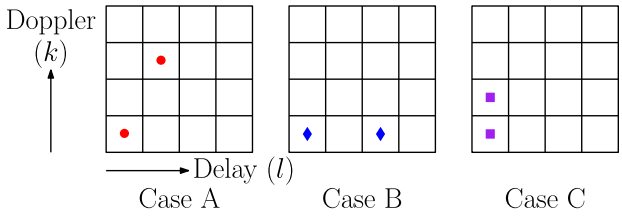

Fig. 1. Examples for the three cases in the diversity analysis for $M = N = 4$.

Finally, the "standard" definition of diversity of OTFS is

$$\rho \triangleq \min_{\mathbf{x}\neq\hat{\mathbf{x}},(\mathbf{x},\hat{\mathbf{x}})} \rho(\mathbf{x},\hat{\mathbf{x}}) = \min_{\mathbf{x}\neq\hat{\mathbf{x}},(\mathbf{x},\hat{\mathbf{x}})} \text{rank}(\mathbf{\Upsilon}(\boldsymbol{\delta})) \tag{7}$$

Observation 2: In matrix $\mathbf{\Xi}_i$ as given in (8), as shown at the bottom of this page, where $0 \le p \le MN - 1$ and $0 \le q \le MN - 1$ [5, Th. 1], the values of n and m can be computed as $n = \lfloor \frac{p}{M} \rfloor$ and $m = p - nM$. Note that $\mathbf{\Xi}_i\boldsymbol{\delta}$ is equivalent to a circulant shift of $\boldsymbol{\delta}$ with some phase shifts. In next section, we derive the diversity order achieved by OTFS system for two channel paths, i.e., $P = 2$.

III. Diversity Analysis for $P = 2$

Without loss of generality, we assume that the two channel paths are located at $(l_1, k_1) = (0, 0)$ and at (l_2, k_2). We divide the diversity analysis of OTFS into the following three cases: *A.* $l_2 \neq 0$ and $k_2 \neq 0$, *B.* $l_2 \neq 0$ and $k_2 = 0$, *C.* $l_2 = 0$ and $k_2 \neq 0$. Fig. 1 describes the examples of the three cases for the OTFS system of $M = N = 4$. Here, the dots represent the delay and Doppler positions of the two channel paths.

A. $l_2 \neq 0$ and $k_2 \neq 0$

Since there are no shifts across the delays or Dopplers due to the first path (i.e., $\mathbf{\Xi}_1 = \mathbf{I}$), the first column of $\mathbf{\Phi}(\boldsymbol{\delta})$ in (5) can be written as

$$\begin{aligned}\mathbf{\Phi_1}(\boldsymbol{\delta}) = \boldsymbol{\delta} = [&\delta_{0,0}, \delta_{1,0}, \ldots, \delta_{M-1,0}, \delta_{0,1}, \delta_{1,1}, \ldots, \delta_{M-1,1}, \\ &\ldots, \delta_{0,N-1}, \delta_{1,N-1}, \ldots, \delta_{M-1,N-1}]^T\end{aligned} \tag{9}$$

where $\delta_{m,n}$ denotes the $m + Mn$ element of $\boldsymbol{\delta}$. The second column of $\mathbf{\Phi}(\boldsymbol{\delta})$ is (l_2, k_2) circulant shifted version of $\mathbf{\Phi_1}(\boldsymbol{\delta})$ with some phase shifts as given in (8). Given that we exclude the case $\boldsymbol{\delta} = 0$ ($\mathbf{x} \neq \hat{\mathbf{x}}$), we have at least one element $\delta_{m,n} \neq 0$ for some m and n. Assume $m \ge l_2$.[1] Let us consider two rows in $\mathbf{\Phi}(\boldsymbol{\delta})$ with $\delta_{m,n}$ as one of the element:

$$\left(\delta_{m,n},\ e^{j2\pi\frac{k_2(m-l_2)}{MN}}\delta_{m-l_2,n-k_2}\right) \tag{10}$$

[1]Note that for $m < l_2$, the expression in (12) will be similar except a phase shift of $e^{-j2\pi\frac{n}{N}}$ in the second term. Assume the value of (12) for $m < l_2$ is zero, i.e., $\delta_{m+l_2,n+k_2} \neq 0$. By repeating (12) for $\delta_{m+l_2,n+k_2}$, we can always get a condition $\delta_{m',n'} \neq 0$, for which $m' > l_2$.

$$\mathbf{\Xi}_i(p,q) = \begin{cases} e^{-j2\pi\frac{n}{N}}e^{j2\pi\frac{k_i([m-l_i]_M)}{MN}}, & \text{if } q = [m-l_i]_M + M[n-k_i]_N \text{ and } m < l_i \\ e^{j2\pi\frac{k_i([m-l_i]_M)}{MN}}, & \text{if } q = [m-l_i]_M + M[n-k_i]_N \text{ and } m \ge l_i \\ 0, & \text{otherwise} \end{cases} \tag{8}$$

$$\left(\delta_{m+l_2,n+k_2},\ e^{j2\pi\frac{k_2(m)}{MN}}\delta_{m,n}\right) \tag{11}$$

The second element in (10) can be made zero by multiplying $\frac{\delta_{m-l_2,n-k_2}}{\delta_{m,n}}e^{j2\pi\frac{k_2(m-l_2)}{MN}}$ by the first column of $\mathbf{\Phi}(\boldsymbol{\delta})$ and subtracting from second column. The second column entry in (11) becomes

$$e^{j2\pi\frac{k_2 m}{MN}}\delta_{m,n} - e^{j2\pi\frac{k_2(m-l_2)}{MN}}\frac{\delta_{m-l_2,n-k_2}}{\delta_{m,n}}\delta_{m+l_2,n+k_2} \tag{12}$$

If we can show that the value in (12) is non-zero for all values of $\delta_{m,n} \neq 0$ and $\boldsymbol{\delta} \subset \mathbf{Z}[j]^{MN\times 1}$, then we can say the two columns of $\mathbf{\Phi}(\boldsymbol{\delta})$ are independent for QAM modulation and we guarantee a diversity order 2, which is the number *P* of paths and hence the maximum achievable value.

The value in (12) becomes zero if

$$\delta^2_{m,n} = e^{-j2\pi\frac{k_2 l_2}{MN}}\delta_{m-l_2,n-k_2}\delta_{m+l_2,n+k_2} \tag{13}$$

If $l_2 \neq 0$ and $k_2 \neq 0$ then the value $e^{-j2\pi\frac{k_2 l_2}{MN}}$ is irrational belonging to the cyclotomic field $\mathbf{Q}(e^{-j2\pi\frac{k_2 l_2}{MN}})$ of degree $\varphi(\min(MN, MN/k_2 l_2)) \geq 2$ for any k_2, l_2 such that $k_2 l_2 < MN/4$ and the above equality cannot be satisfied by $\delta_{m,n} \neq 0$ and $\boldsymbol{\delta} \subset \mathbf{Z}[j]^{MN\times 1}$ (here $\varphi(n)$ denotes the Euler totient function, counting the number of relatively primes to *n*, and the second argument of the min only applies for $k_2 l_2$ dividing *MN*).

Since the typical wireless channels are underspread, i.e., $l_2 \ll M, k_2 \ll N$, for $P = 2$ paths at (0, 0) and (l_2, k_2) with $l_2 \neq 0$ and $k_2 \neq 0$, we have diversity order 2.

Example: For $M = N = 4$ and $k_2 = l_2 = 1$, the condition in (12) becomes

$$\delta^2_{m,n} = e^{-j\pi\frac{1}{8}}\delta_{m-l_2,n-k_2}\delta_{m+l_2,n+k_2} \tag{14}$$

Since (14) cannot be satisfied for $\delta_{m,n} \neq 0$ and $\boldsymbol{\delta} \subset \mathbf{Z}[j]^{MN\times 1}$, we have diversity order of 2.

Special Case: For $M = N = 2$ and $k_2 = l_2 = 1$, the conditions in (10) and (11) becomes

$$\delta^2_{m,n} = -j\delta^2_{[m-l_2]_M,[n-k_2]_N} \text{ (or) } \delta^2_{m,n} = j\delta^2_{[m-l_2]_M,[n-k_2]_N}$$

However, for $\delta_{m,n} \neq 0$ and $\boldsymbol{\delta} \subset \mathbf{Z}[j]^{MN\times 1}$, neither one of the above conditions can be satisfied, which yields full diversity.

B. $l_2 \neq 0$ and $k_2 = 0$

Let us rewrite the $\mathbf{\Phi}(\boldsymbol{\delta})$ in (5) as follows:

$$\mathbf{\Phi}(\boldsymbol{\delta}) = \begin{bmatrix}\Xi_1 & \Xi_2\end{bmatrix}\begin{bmatrix}\boldsymbol{\delta} & \mathbf{0}\\ \mathbf{0} & \boldsymbol{\delta}\end{bmatrix} \tag{15}$$

Now, from (15), $\mathbf{\Upsilon}(\delta)$ can be written in the form

$$\mathbf{\Upsilon}(\delta) = \mathbf{\Phi}^\dagger(\boldsymbol{\delta})\mathbf{\Phi}(\boldsymbol{\delta}) = \begin{bmatrix}\boldsymbol{\delta}^\dagger\boldsymbol{\delta} & \boldsymbol{\delta}^\dagger\mathbf{\Lambda}\boldsymbol{\delta}\\ \boldsymbol{\delta}^\dagger\mathbf{\Lambda}^\dagger\boldsymbol{\delta} & \boldsymbol{\delta}^\dagger\boldsymbol{\delta}\end{bmatrix} \tag{16}$$

where $\mathbf{\Lambda} \triangleq \Xi_1^\dagger\Xi_2$, and we use the fact that $\Xi_1^\dagger\Xi_1 = \Xi_2^\dagger\Xi_2 = \mathbf{I}$. For $k_2 = 0, l_2 \neq 0$, $\mathbf{\Lambda}$ can be written as

$$\mathbf{\Lambda} = (\mathbf{F}_N^\dagger \otimes \mathbf{I}_M)^\dagger\mathbf{\Pi}^{l_2}(\mathbf{F}_N^\dagger \otimes \mathbf{I}_M) \tag{17}$$

Therefore, the determinant of $\mathbf{\Upsilon}(\delta)$ is equal to

$$\det[\mathbf{\Upsilon}(\delta)] = |\boldsymbol{\delta}^\dagger\boldsymbol{\delta}|^2 - |\boldsymbol{\delta}^\dagger\mathbf{\Lambda}\boldsymbol{\delta}|^2 \tag{18}$$

$$= |\hat{\boldsymbol{\delta}}^\dagger\hat{\boldsymbol{\delta}}|^2 - |\hat{\boldsymbol{\delta}}^\dagger\mathbf{\Pi}^{l_2}\hat{\boldsymbol{\delta}}|^2 \tag{19}$$

where $\hat{\boldsymbol{\delta}} = (\mathbf{F}_N^\dagger \otimes \mathbf{I}_M)\boldsymbol{\delta}$. From (19) and (7), using Cauchy-Schwarz inequality, we can see that OTFS achieves rank 1 only when

$$\hat{\boldsymbol{\delta}} = e^{j\theta}\mathbf{\Pi}^{l_2}\hat{\boldsymbol{\delta}} \tag{20}$$

for some angle θ. For simplicity, we assume l_2 divides *M*. Through simple algebraic computations, the condition in (20) can be written as

$$\hat{\boldsymbol{\delta}}(r) = e^{j\theta}\hat{\boldsymbol{\delta}}([r - l_2]_M),\ \text{for } 0 \leq r \leq MN-1, \tag{21}$$

where θ is of the form $2\pi\frac{l_2}{MN}c$, for any $c \in \mathbf{Z}$. As $\boldsymbol{\delta} = (\mathbf{F}_N^\dagger \otimes \mathbf{I}_M)^\dagger\hat{\boldsymbol{\delta}} = (\mathbf{F}_N \otimes \mathbf{I}_M)\hat{\boldsymbol{\delta}}$, from (21), the value of $\boldsymbol{\delta}$ becomes

$$\begin{aligned}&[\delta_{m,0}, \delta_{m,1}, \ldots, \delta_{m,N-1}]^T\\ &= \mathbf{F}_N\left[e^{jp\theta}\hat{\boldsymbol{\delta}}(q), e^{jp\theta}e^{j\frac{M}{l_2}\theta}\hat{\boldsymbol{\delta}}(q), \ldots, e^{jp\theta}e^{j\frac{M}{l_2}(N-1)\theta}\hat{\boldsymbol{\delta}}(q)\right]^T\\ &= e^{jp\theta}\hat{\boldsymbol{\delta}}(q)[0, \ldots, \underbrace{1}_{(c'+1)^{th}\text{ entry}}, 0, \ldots, 0]^T\end{aligned} \tag{22}$$

where $p = \lfloor m/l_2 \rfloor$, $q = [m]_{l_2}$, $0 \leq m \leq M-1$, and $c' = [c]_N$. Therefore, the entries of $\boldsymbol{\delta}$ can be written as

$$\delta_{m,n} = \begin{cases} e^{jp\theta}\delta_{q,c'+1}, & \text{if } n = c'+1\\ 0, & \text{otherwise}\end{cases} \tag{23}$$

for $0 \leq m \leq M-1$. However, as $\delta_{m,n} \in \mathbf{Z}[j]$, from (23) we can derive that $e^{jp\theta} \in \mathbf{Z}[j]$, which is possible only when $e^{j\theta}$ takes values from the set $\{+1, -1, +j, -j\}$.

Example 1: Consider $M = 2, N = 2, l_2 = 1, k_2 = 0$ and 4-QAM modulation. The following are some of the $\boldsymbol{\delta}$ patterns that yield rank 1:

$$[2,2,0,0]^T, [2,-2,0,0]^T, [-2,2,0,0]^T, [-2,-2,0,0]^T,$$
$$[0,0,2,2j]^T, [0,0,2j,-2]^T, [0,0,-2,2j]^T, [0,0,-2,-2j]^T$$

We can clearly see that all the above patterns follow the structure in (23).

1) Upper Bound on the Number of Pairs Yielding Rank 1: From (23), for a given $\mathbf{x}$, the maximum number of $\hat{\mathbf{x}}$ that yield rank 1 can be computed as $4N(Q^{l_2}-1)$, where *N* denotes the all possible values of c', $(Q^{l_2}-1)$ is the number of possible selection of QAM symbols for a given c' which is due to $0 \leq q \leq l_2 - 1$, and 4 is due to the set $\{+1, -1, +j, -j\}$.

For the case of l_2 not dividing *M*, the value of l_2 in the condition (21) is replaced by $l_2' = \gcd(l_2, M)$.

C. $l_2 = 0$ and $k_2 \neq 0$

For the case of $l_2 = 0$ and $k_2 \neq 0$, the value of $\mathbf{\Lambda}$ in (16) becomes

$$\mathbf{\Lambda} = (\mathbf{F}_N^\dagger \otimes \mathbf{I}_M)^\dagger\mathbf{\Delta}^{k_2}(\mathbf{F}_N^\dagger \otimes \mathbf{I}_M) \tag{24}$$

Now, the determinant of $\mathbf{\Upsilon}(\delta)$ can be written as

$$\det[\mathbf{\Upsilon}(\delta)] = |\hat{\boldsymbol{\delta}}^\dagger\hat{\boldsymbol{\delta}}|^2 - |\hat{\boldsymbol{\delta}}^\dagger\mathbf{\Delta}^{k_2}\hat{\boldsymbol{\delta}}|^2 \tag{25}$$

where $\hat{\boldsymbol{\delta}} = (\mathbf{F}_N^\dagger \otimes \mathbf{I}_M)\boldsymbol{\delta}$. Therefore, using Cauchy-Schwarz inequality, we can see that OTFS achieves rank 1 only when

$$\hat{\boldsymbol{\delta}} = e^{j\theta}\mathbf{\Delta}^{k_2}\hat{\boldsymbol{\delta}} \tag{26}$$

for some angle θ. For simplicity, we assume k_2 divides N. Assuming $\hat{\boldsymbol{\delta}}(r) \neq 0$ for some $0 \leq r \leq MN-1$, from (26), we can obtain the conditions on $\hat{\boldsymbol{\delta}}$ as

$$\hat{\boldsymbol{\delta}}(r') = 0 \text{ for } [r'-r]_{\frac{MN}{k_2}} \neq 0 \tag{27}$$

That is, $\hat{\boldsymbol{\delta}}$ contains at the most k_2 non-zero elements separated by $\frac{MN}{k_2}$. Now, similar to (22), the value of $\boldsymbol{\delta}$ can be written as

$$\begin{aligned}&[\delta_{m,0}, \delta_{m,1}, \ldots, \delta_{m,N-1}]^T \\ &= \mathbf{F}_N \left[\hat{\boldsymbol{\delta}}(m), \hat{\boldsymbol{\delta}}(m+M), \ldots, \hat{\boldsymbol{\delta}}(m+(N-1)M)\right]^T\end{aligned} \tag{28}$$

From (27), we can immediately see that the vector in (28) can have at the most k_2 non-zero elements for one value of m, $0 \leq m \leq M-1$, and all zero elements for all other m.

Example 2: Consider $M=2$, $N=2$, $l_2=0, k_2=1$ and 4-QAM modulation. As $k_2=1$, only one element in (28) can be non-zero for some value of $m=m'$. Therefore, the entries of $\boldsymbol{\delta}$ can be written as

$$\delta_{m,n} = \begin{cases} e^{-j2\pi\frac{nc}{N}}\delta_{m',n}, & \text{if } m=m' \\ 0, & \text{otherwise} \end{cases} \tag{29}$$

for $0 \leq n, c \leq N-1$. The following are some of the $\boldsymbol{\delta}$ patterns that yield rank 1:

$$\begin{aligned}&[2,0,2,0]^T, [-2,0,-2,0]^T, [-2,0,2,0]^T, [2,0,-2,0]^T, \\ &[0,-2j,0,2j]^T, [0,2j,0,2j]^T, [0,2j,0,-2j]^T, [0,2,0,-2]^T,\end{aligned}$$

We can clearly see that all the above patterns follow the structure in (29).

1) Upper Bound on the Number of Pairs Yielding Rank 1: From (28), for a given $\mathbf{x}$, the maximum number of $\hat{\mathbf{x}}$ yielding rank 1 can be computed as $M\frac{N}{k_2}(Q^{k_2}-1)$, where M denotes the all possible values of m, $(Q^{k_2}-1)$ is the number of possible selection of QAM symbols for a given m which is due to the k_2 non-zero elements in (28), and $\frac{N}{k_2}$ is the possible k_2 non-zero sets in (28). For the case of k_2 not dividing N, the value of k_2 in (27) is replaced by $k_2' = \gcd(k_2, N)$ and $\hat{\boldsymbol{\delta}}$ can contain at the most k_2' non-zero elements.

D. Diversity for the Three Cases Above

Summarizing our analysis of the three cases above, an upper bound $\mathcal{N}(\mathbf{x}, \hat{\mathbf{x}})$ to the number of pairs $(\mathbf{x}, \hat{\mathbf{x}})$ yielding rank 1 is

$$\mathcal{N}(\mathbf{x}, \hat{\mathbf{x}}) = \begin{cases} 0, & \text{if } l_2 \neq 0, k_2 \neq 0 \\ 4N(Q^{l_2'}-1)Q^{MN}, & \text{if } l_2 \neq 0, k_2 = 0 \\ M\frac{N}{k_2'}(Q^{k_2'}-1)Q^{MN}, & \text{if } l_2 = 0, k_2 \neq 0 \end{cases} \tag{30}$$

Now, consider the ratio of $\mathcal{N}(\mathbf{x}, \hat{\mathbf{x}})$ to the total number of possible pairs $\mathcal{T}(\mathbf{x}, \hat{\mathbf{x}}) = Q^{MN}(Q^{MN}-1)$. we obtain

$$\mathcal{R}(\mathbf{x}, \hat{\mathbf{x}}) = \frac{\mathcal{N}(\mathbf{x}, \hat{\mathbf{x}})}{\mathcal{T}(\mathbf{x}, \hat{\mathbf{x}})} \approx \begin{cases} 0, & \text{if } l_2 \neq 0, k_2 \neq 0 \\ \frac{4N}{Q^{(MN-l_2')}}, & \text{if } l_2 \neq 0, k_2 = 0 \\ \frac{MN}{k_2' Q^{(MN-k_2')}}, & \text{if } l_2 = 0, k_2 \neq 0 \end{cases} \tag{31}$$

As $l_2 \ll M, k_2 \ll N$, we can see that, as M and N grow larger, $\mathcal{R}(\mathbf{x}, \hat{\mathbf{x}})$ quickly approaches zero.

$$\mathcal{R}(\mathbf{x}, \hat{\mathbf{x}}) \xrightarrow{M,N\to\infty} 0 \tag{32}$$

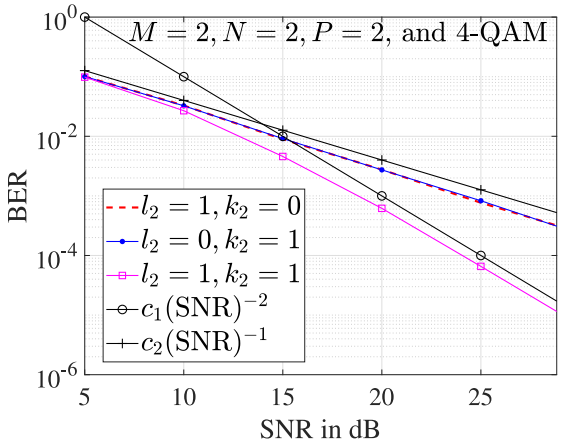

Fig. 2. BER of OTFS for different (l_2, k_2) with $M=2$, $N=2$, $P=2$, and 4-QAM.

Example 3: Consider $M=16$, $N=16$, $l_2=4, k_2=0$, and 4-QAM modulation. Then the value of $\mathcal{R}(\mathbf{x}, \hat{\mathbf{x}})$ is $\approx 10^{-150}$.

Now, consider again the union bound to P_e, as shown in (6). Each individual term in sum (6) can be viewed as a function of SNR whose slope is essentially dictated by the value of $\rho(\mathbf{x}, \hat{\mathbf{x}})$. As SNR increases, the terms with higher values of $\rho(\mathbf{x}, \hat{\mathbf{x}})$ become increasingly less relevant to determine the value of P_e, so that for very high SNR the only significant terms in (6) are those with the lowest value of $\rho(\mathbf{x}, \hat{\mathbf{x}})$. This justifies the use of the standard definition (7) of diversity ρ, useful for very high SNR. For intermediate values of SNR, however, the use of standard diversity might not be appropriate whenever the number of terms in (6) with exponent higher than ρ is *much greater* than the number of those with exponent ρ. If this is the case, for those values of SNR the slope of the union-bound curve might be dictated by an exponent higher than ρ. We call this exponent "effective diversity." In our context, OTFS achieves full effective diversity with typical system parameters as $P=2$. Future work will show the extension of the above analysis to P values greater than 2.

Remark 1: Note that the above diversity analysis differs from the work in [8] in two aspects.

1) The diversity analysis in [8] is proposed only for the ideal biorthogonal waveforms that satisfy both time and frequency orthogonality conditions, which is not practically feasible due to Heisenberg's uncertainty principle. Instead, the analysis in this letter assumes feasible rectangular waveforms, which yield different input–output relations (extra phase shifts in (8)) compared to the ideal waveforms [5], [8]. Moreover, our analysis developed for rectangular waveforms can be straightforwardly extended to any arbitrary waveforms, for example, raised cosine waveforms [5].
2) The work in [8] showed that the standard diversity order of the OTFS system is one and proposed a phase rotation based precoding scheme to achieve full diversity. However, in this letter, we show that, with sufficiently large M and N, the OTFS system achieves full effective diversity, thus any precoding schemes are not required.

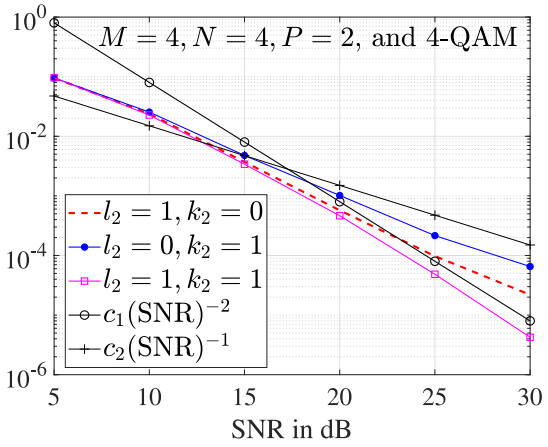

Fig. 3. BER of OTFS for different (l_2, k_2) with $M = 4$, $N = 4$, $P = 2$, and 4-QAM.

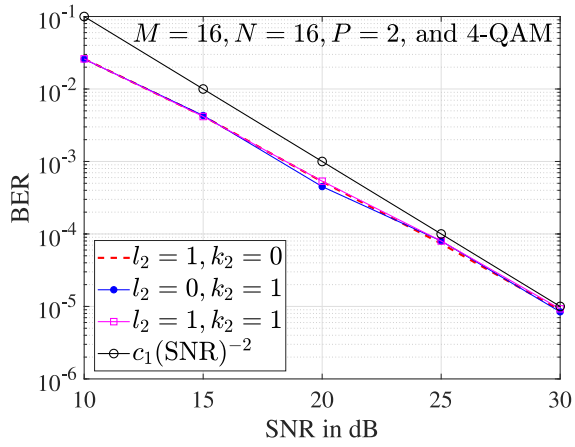

Fig. 4. BER of OTFS for different (l_2, k_2) with $M = 16$, $N = 16$, $P = 2$, and 4-QAM.

IV. Simulation Results

In this section, we present the BER of OTFS for different choices of system parameters. We consider $P = 2$, $l_1 = 0, k_1 = 0$, and 4-QAM modulation in all the simulations. The path coefficients are $h_1, h_2 \sim \mathcal{CN}(0, 1/2)$. Figs. 2, 3, and 4 show the BER of OTFS for different (l_2, k_2) with ($M = 2$, $N = 2$), ($M = 4$, $N = 4$), and ($M = 16$, $N = 16$) respectively. We use the optimal ML detector in Figs. 2 and 3 and the message passing detector [7] in Fig. 4. Note that the plots of $c_1(\mathrm{SNR})^{-2}$ and $c_2(\mathrm{SNR})^{-1}$ are only used to identify the slope of the curves, and do not represent an upper bound. From the figures, we can observe that:

i) In all the three cases, OTFS achieves the full diversity of two with the second path located at $l_2 = 1, k_2 = 1$. This is due to the absence of rank 1 pairs if $k_2 \neq k_1$ and $l_2 \neq l_1$.

ii) OTFS achieves rank 1 with the second paths located at $l_2 = 1, k_2 = 0$ or $l_2 = 0, k_2 = 1$ for ($M = 2$, $N = 2$) and ($M = 4$, $N = 4$). This is because of the upper bound in (30) is significant for these system parameters. However, we can see that the diversity change happens at a higher SNR with ($M = 4$, $N = 4$) compared to the case of ($M = 2$, $N = 2$).

iii) Finally, independent of the second path location, OTFS achieves the same performance for ($M = 16$, $N = 16$) for the BER ranges up to 10^{-5}. This is justified by the small number of rank-1 pairs as mentioned in Example 3.

From the above observations, we conclude that OTFS system achieves full effective diversity for sufficiently large values of M and N.

V. Conclusion

We have analyzed the diversity of OTFS over two-path channels. After deriving an upper bound on the number of pairs that prevent the achievement of full rank, we have shown that the number of these pairs is relatively vanishingly small for sufficiently large values of M and N (e.g., $M = N = 16$). Through analysis and simulations, we can conclude that, even though the theoretical diversity of OTFS is one, effective diversity, which takes value 2, is the significant parameter expressing error performance.

References

[1] E. Biglieri, *Coding for Wireless Channels*. New York, NY, USA: Springer, 2005.

[2] R. Hadani *et al.*, "Orthogonal time frequency space modulation," in *Proc. IEEE WCNC*, San Francisco, CA, USA, 2017, pp. 1–6.

[3] R. Hadani *et al. Orthogonal Time Frequency Space Modulation*. Accessed: Aug. 1, 2018. [Online]. Available: https://arxiv.org/pdf/1808.00519.pdf

[4] R. Hadani and A. Monk, "OTFS: A new generation of modulation addressing the challenges of 5G," Santa Clara, CA, USA, Cohere Technol., OTFS Physics White Paper, 2018. [Online]. Available: https://arxiv.org/pdf/1802.02623.pdf

[5] P. Raviteja, Y. Hong, E. Viterbo, and E. Biglieri, "Practical pulse-shaping waveforms for reduced-cyclic-prefix OTFS," *IEEE Trans. Veh. Technol.*, vol. 68, no. 1, pp. 957–961, Jan. 2019.

[6] E. Biglieri, P. Raviteja, and Y. Hong, "Error performance of orthogonal time frequency space (OTFS) modulation," in *Proc. IEEE ICC Workshop*, Shanghai, China, 2019, pp. 1–6.

[7] P. Raviteja, K. T. Phan, Y. Hong, and E. Viterbo, "Interference cancellation and iterative detection for orthogonal time frequency space modulation," *IEEE Trans. Wireless Commun.*, vol. 17, no. 10, pp. 6501–6515, Oct. 2018.

[8] G. D. Surabhi, R. M. Augustine, and A. Chockalingam, "On the diversity of uncoded OTFS modulation in doubly-dispersive channels," *IEEE Trans. Wireless Commun.*, vol. 18, no. 6, pp. 3049–3063, Jun. 2019.

[9] K. R. Murali and A. Chockalingam, "On OTFS modulation for high-doppler fading channels," in *Proc. ITA*, San Diego, CA, USA, 2018, pp. 1–10.

[10] L. Li *et al. A Simple Two-Stage Equalizer With Simplified Orthogonal Time Frequency Space Modulation Over Rapidly Time-Varying Channels*. Accessed: Sep. 8, 2017. [Online]. Available: https://arxiv.org/abs/1709.02505

[11] T. Zemen, M. Hofer, D. Loeschenbrand, and C. Pacher, "Iterative detection for orthogonal precoding in doubly selective channels," in *Proc. IEEE 29th Annu. Int. Symp. PIMRC*, Bologna, Italy, 2018, pp. 1–7.

[12] A. Farhang, A. RezazadehReyhani, L. E. Doyle, and B. Farhang-Boroujeny, "Low complexity modem structure for OFDM-based orthogonal time frequency space modulation," *IEEE Wireless Commun. Lett.*, vol. 7, no. 3, pp. 344–347, Jun. 2018.

[13] A. RezazadehReyhani, A. Farhang, M. Ji, R. R. Chen, and B. Farhang-Boroujeny, "Analysis of discrete-time MIMO OFDM-based orthogonal time frequency space modulation," in *Proc. IEEE ICC*, Kansas City, MO, USA, 2018, pp. 1–6.

[14] V. Khammammetti and S. K. Mohammed, "OTFS-based multiple-access in high doppler and delay spread wireless channels," *IEEE Wireless Commun. Lett.*, vol. 8, no. 2, pp. 528–531, Apr. 2019.